A.C. Conductivity and Electric Modulus Studies of $LiNi_{1/3}Mn_{1/3}Co_{1/3}O_2$ Cathode Thin Films Grown by Pulsed Laser Deposition Technique

Kamatam Hari Prasad [a,b], Ratnakar Arumugam [a,c], E.S. Srinadhu [d], N. Satyanarayana [a, *]

[a]Department of Physics, Pondicherry University, Puducherry – 605014, India.
[b] Institute of Aeronautical Engineering, Dundigal, Hyderabad – 500 043, India.
[c] Centre for Nanoscience and Technology, Pondicherry University, Puducherry – 605014, India.
[d] LAM Research Corporation, Fremont, CA, 94538, USA
[*]Corresponding author. Tel: 0413-2654404; E-mail: nallanis2011@gmail.com

ABSTRACT

Layer structured $LiNi_{1/3}Co_{1/3}Mn_{1/3}O_2$ (LNMCO) thin films were grown on the Ti/(Si) (100) substrate by pulsed laser deposition technique under different oxygen partial pressures (from 50 mTorr to 300 mTorr) by keeping the substrate temperature at 500 ºC. X-ray diffraction pattern of the LNMCO thin film annealed under 300 mTorr showed the formation of pure rhombohedral phase. AFM micrographs of LNMCO thin films reveal the surface morphology and roughness. The measured impedance data of all the prepared LNMCO thin films grown under different oxygen partial pressures were analyzed using the win fit software and evaluated the ac conductivity, dielectric constant (ε′) and electric modulus as a function as a function of frequency. From the observed results, the developed LNMCO thin film grown under 300 mTorr can be a better cathode material for developing all-solid-state rechargeable lithium-ion micro-batteries.

Keywords: $LiNi_{1/3}Co_{1/3}Mn_{1/3}O_2$ thin films; Pulsed laser deposition; ac conductivity; electric modulus.

1 INTRODUCTION

Recent developments in all-solid-state thin film micro-batteries have attracted enormous interest due to their potential applications as power sources for micro- and nanodevices such as smart cards, implantable medical devices, complementary metal oxide semiconductors (CMOS), memory chips, micro-electro-mechanical systems (MEMS), nano-electro-mechanical systems (NEMS) [1-6]. Cathode, anode, and electrolyte materials are the major parts of the lithium batteries, of which, cathode material plays an important role in lithium battery technology. Recently, $LiNi_{1/3}Co_{1/3}Mn_{1/3}O_2$, which is composed of divalent Ni, tetravalent Mn, and trivalent Co, has received considerable attention due to high capacity associated with the $Ni^{2+/4+}$ and $Co^{3+/4+}$ redox couples and its thermal and structural properties supported by tetravalent Mn and also, it is superior to the conventional $LiCoO_2$. The $LiNi_{1/3}Mn_{1/3}Co_{1/3}O_2$ (LNMCO) is the most widely used cathode materials in lithium-ion battery technology, due to its advantages of exhibiting high energy density, high discharge capacity, good reversibility during the oxidation and reduction process, etc. Thus, $LiNi_{1/3}Mn_{1/3}Co_{1/3}O_2$ is considered as a promising cathode material for all-solid-state thin film lithium batteries application. Many deposition methods such as chemical vapor, spray pyrolysis, RF magnetron sputtering (RFMS) [7-10], pulsed laser deposition, etc., techniques, have been used for the fabrication of thin film electrodes.

In the present paper, lithium-rich layer-structured $LiNi_{1/3}Co_{1/3}Mn_{1/3}O_2$ (LNMCO) thin films were grown on the silicon (Si) (100) substrate by pulsed laser deposition technique under different oxygen partial pressures (from 50 mTorr to 300 mTorr) by keeping the substrate temperature at 500 ºC. Crystalline phase and surface morphology of all the grown LNMCO thin films were investigated by using X-ray diffraction (XRD), and atomic force microscopy (AFM) respectively. Also, ac conductivity, dielectric constant (ε′) and electric modulus properties of all the prepared LNMCO thin films were evaluated by analyzing the measured impedance data using the Win Fit software.

2. EXPERIMENTAL TECHNIQUES

2.1 Preparation of LNMCO Thin Films

The $LiNi_{1/3}Co_{1/3}Mn_{1/3}O_2$ thin films were grown on Ti/Si (100) substrate by the pulsed laser deposition (PLD) technique. Before ablation, surface contaminations were removed from the Si (100) substrates using H_2SO_4:H_2O_2:H_2O (4:1:1) solution by etching for the 30 seconds and subsequent rinsing by de-ionized water and methanol cleaning. The cleaned substrate was mounted on a substrate holder having the heating arrangement. The $LiNi_{1/3}Co_{1/3}Mn_{1/3}O_2$ target with 99.99% purity (procured from Testbourne Pvt. Ltd., USA) was ablated using a KrF excimer laser (Lambda Physik, Germany model COMPEX-201, wavelength (λ) =248 nm, Pulse width = 25 ns). The energy density of the pulses was approximately 2 J/cm^2 with a laser spot of 2 mm ×1 mm on the target. The target-to-substrate separation was 30 mm. Laser light irradiated

the target at an angle of 50° with respect to the surface normal, while Si (100) substrates were placed in the direction of target normal. The deposition chamber, which was then evacuated to the base pressure of 2×10^{-6} Torr. The LNMCO thin films were grown on Si (100) substrate under different oxygen partial pressures (i.e. 50 m Torr, 200 mTorr, and 300 mTorr). The depositions were carried out at 500 °C for 2 hours under different oxygen partial pressures at a pulse frequency of 10 Hz. The substrate temperature was monitored using a K-type thermocouple attached to the substrate holder and kept between two Si pieces. The thickness of the film measured by a stylus profilometer (Ambios, USA).

2.2 Characterization

XRD patterns of LNMCO films were recorded using the PANalytical, Philips, X' Pert Pro X-ray diffractometer having monochromatic X-ray source of CuK_α radiation with a wavelength (λ) of 1·541060 Å, operated at 40 kV and 30 mA. Atomic Force Microscopy (AFM) images of the LNMCO films were recorded using the NanoScope -V Multimode™ SPM, Veeco Instruments. The AFM was operated in tapping mode (non-contact) to prevent the damage to the films and also to provide optimal image and quality data. Using Nanoscope analysis software, the observed 3-D AFM images of the LNMCO thin films were analyzed and obtained the grain shape, size and surface roughness parameters like root mean square (RMS) roughness (R_q), average surface roughness (R_a). The maximum height asymmetries values of surface skewness and kurtosis are determined using WSxM 8.0 develop 5.3 software. Impedance measurements were made on LNMCO cathode thin films of the following configuration [Cu/(LNMCO/Ti/Si (100))/Cu] for the as-deposited and post-annealed samples at different temperatures in the frequency range from 100 Hz to 10 MHz using Alpha A high-performance frequency analyzer of Novocontrol, Germany. The measured impedance data and the dimensions of LNMCO thin films were used for calculating AC conductivity (σ_{ac}), and electric modulus (M′) of LNMCO thin films.

3. RESULTS AND DISCUSSION

3.1 XRD

Fig.1 shows the X-ray diffraction patterns of LNMCO thin films grown at different oxygen partial pressures along with the JCPDS data. From fig. 1, it is observed that the oxygen partial pressure at 50 m Torr grown LNMCO thin film exhibits one low-intensity XRD peak, marked as #, is due to the pristine phase of Ti/Si (100) orientation film. The oxygen partial pressure at 50 mTorr grown LNMCO thin film showed peak free XRD pattern, which confirms the formation of the amorphous phase of LNMCO thin film. XRD patterns of the LNMCO thin films grown under oxygen partial pressures at 200 mTorr and 300 mTorr showed (0 0 3) and (1 0 4) predominant XRD peaks and (1 0 1), (0 1 2), (0 1 5), and (1 0 7) are relatively weak intensity peaks. The X-ray diffraction peak, especially (104) plane, became sharper with the increase of oxygen partial pressure. From fig.1 the XRD pattern of the LNMCO thin film grown under oxygen partial pressure at 300 mTorr is in good agreement with the JCPDS (card no. 01-075-0532) data of a rhombohedral layer structure.

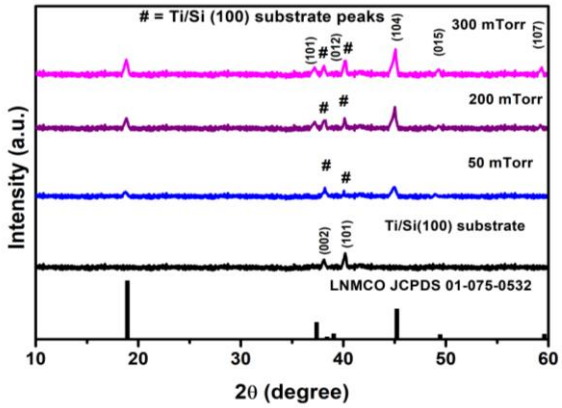

Fig. 1 X-ray diffraction patterns of LNMCO thin films grown under different oxygen partial pressures along with the JCPDS data.

3.2 AFM

Fig. 2. [a, b, and c] shows the three-dimensional (3D) AFM images of LNMCO thin films grown under different oxygen partial pressures. From fig. 2. [a, b, and c], the AFM images clearly showed that the grain size increases with the increase of oxygen partial pressure. From fig. 2 [a], the 3D AFM image of the LNMCO thin film shows the smaller individual grains with lower roughness. From fig. 2. [b], and [c], the 3D AFM images of the LNMCO thin films grown under oxygen partial pressures at 200 mTorr, and 300 mTorr showed denser granular structure, and it is also observed that there is a decrement in the separation between the grains and grain boundary with the increase of oxygen partial pressure. From the AFM images, the grain size, R_a, R_q and height asymmetry values evaluated using Nanoscope analysis software are presented in table 1. From table 1, the observed the grain sizes are found to be 142 nm, 175 nm, and 203 nm, respectively for the LNMCO thin films grown under different oxygen partial pressures of 50 m Torr, 200 mTorr, and 300 mTorr, which indicate that the grain size increases with increase of oxygen partial pressure [11]. The grain size plays an important role in the electrochemical performance of Li-ion batteries, because, the small grain size can provide a large specific surface area, shorter Li-ion diffusion path, which helps to migrate

Li-ions easily in the LNMCO. From table 2, it is also found that the LNMCO thin film grown under 300 mTorr oxygen partial pressure has the highest surface roughness (R_a: 18.23 nm and R_q: 19.37 nm) and the LNMCO thin film grown under 50 mTorr oxygen partial pressure has the lowest surface roughness (R_a of 7.94 nm and R_q of 11.78 nm).

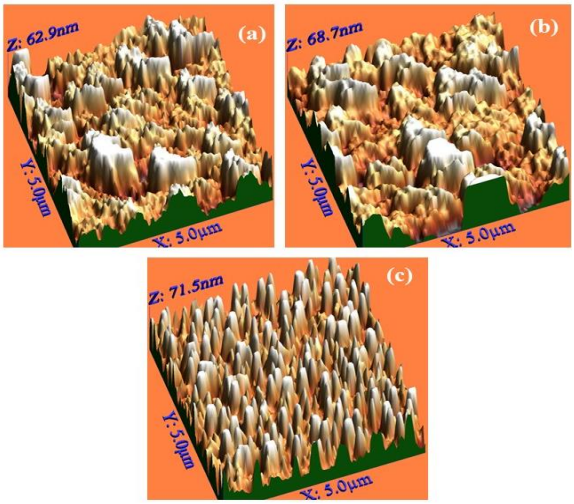

Fig. 2 2-dimensional and 3-dimensional AFM micrographs of the LNMCO thin films grown under [a] 50 m Torr, [b] 200 mTorr, and [c] 300 mTorr.

Table 1. Summarizing AFM surface roughness parameters of $LiNi_{1/3}Co_{1/3}Mn_{1/3}O_2$ thin films (5 µm × 5 µm) grown under different oxygen partial pressures of 50 m Torr, 200 mTorr, and 300 mTorr.

Oxygen pressures (mTorr)	Average roughness (nm) R_a	RMS roughness (nm) R_q	Maximum Height (nm) R_{max}	AFM grain size (nm)
50	7.94	11.78	65.5	142
200	10.35	13.99	68.7	175
300	18.23	19.37	71.5	203

3.3 AC Conductivity (σ_{ac})

Fig. 3 shows the AC conductivity versus frequency plots obtained at 298 K of LNMCO thin films grown under different pressures by keeping the substrate temperature at 500 °C. From fig. 3, the frequency dependent conductivity plots showed two distinct regions within the measured frequency window, (i) the low-frequency plateau region and (ii) high-frequency dispersion region. The plateau region corresponds to frequency independent conductivity $\sigma_{(0)}$ or dc conductivity (σ_{dc}) and it is evaluated by extrapolating the plateau region to the zero frequency (Y-axis). The frequency independent conductivity may be attributed to the long-range transport of free charge carriers with the applied field in LNMCO thin films. The observed a.c. conductivity in the high-frequency dispersion region follows Jonscher's universal power law (JUPL).

$$\sigma_{(\omega)} = \sigma_{(0)} + A\omega^s \quad (1)$$

where, $\sigma_{(\omega)}$ is the ac conductivity, $\sigma_{(0)}$ is the zero frequency limit of $\sigma_{(\omega)}$, A is a constant, and s is the power law exponent ($0 < s < 1$). From fig. 3, it can be observed that the frequency at which the dispersion region deviated from the plateau is defined as the hopping frequency (ω_p), where, the relaxation effects starts. Also, it can be observed that the hoping frequency moved towards the higher frequency with the increase of pressure in the LNMCO thin film. From fig. 3, the observed dispersion region of conductivity is may be due to hopping of electrons between adjacent sites, results in local displacement of charge carriers in the direction of the applied frequency and hence, it may follow the diffusion controlled relaxation (DCR) model [12-16].

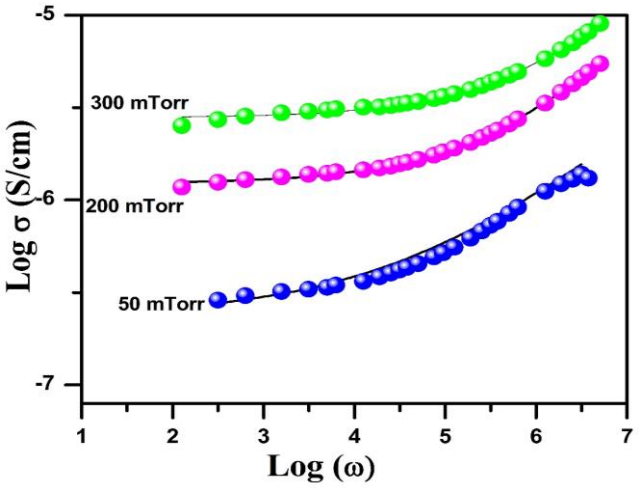

Fig. 3 Log (σ_{ac}) vs. Log (ω) plots obtained plots obtained at 298 K of LNMCO thin films grown under different oxygen partial pressures by keeping the substrate temperature at 500 °C.

3.4 Electric Modulus (M'')

Fig. 4. shows the imaginary part of the electric modulus (M'') versus log(ω) plots obtained at room temperature of LNMCO thin films grown under different oxygen partial pressures by keeping the substrate temperature at 500 °C. From fig. 4, the imaginary part of electric modulus (M'') versus log (ω) exhibit the peak at the relaxation frequency maximum (f_{max}) and its frequency position shifts towards higher frequency regions and it is also observed that the broadness of the electric modulus (M'') versus log (ω) curve increases with increase in oxygen partial pressure. The relaxation frequency maximum (f_{max}) peaks shift towards the higher frequency region with the increase of oxygen partial pressure, which can be attributed to the variation of

relaxation time (τ) of the charge carriers and it is found to exhibit non-Debye type behavior in the LNMCO thin film sample [12-16].

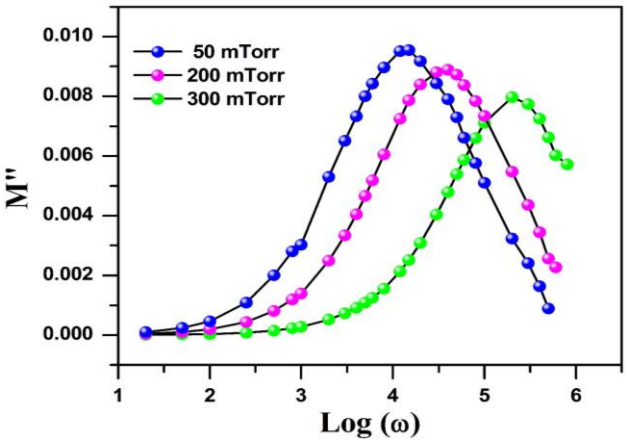

Fig. 4. The imaginary part of the electric modulus (M") versus log(ω) plots obtained at 298 K of LNMCO thin films grown under different oxygen partial pressures by keeping the substrate temperature at 500 ºC.

4 CONCLUSION

Nanocrystalline layer-structured LNMCO thin films were grown on the Ti/silicon (Si) (100) substrate by pulsed laser deposition technique grown under different oxygen partial pressures by keeping the substrate temperature at 500 ºC. The phase purity of the LNMCO films was confirmed by the X-ray diffraction result. The surface morphology and roughness of the LNMCO films were obtained from AFM results. The measured impedance data of all the prepared LNMCO thin films under different oxygen partial pressures were analyzed using the win fit software and evaluated the ac conductivity, dielectric constant (ε′) and electric modulus as a function of frequency. From the observed results, the developed LNMCO thin film grown under 300 mTorr can be a better cathode material for developing all-solid-state rechargeable lithium-ion micro-batteries.

ACKNOWLEDGMENT

NS would like to thank the DST-Nano mission, Govt. of India, for providing grants in the form of research project sanction letter No.: SR/S5/NS-49/2005, dated on 30-07-2010 and NRB-DRDO, Govt. of India, for providing grants in the form of research project sanction letter No.: NRB-377/MAT/16-17, dated on 19-04-2016, respectively for developing five targets DC/RF magnetron sputtering system and electrochemical system facilities for developing and characterizing all solid-state thin film lithium-ion micro-batteries.

REFERENCES

[1] J. M. Tarascon, M. Armand, Nature, 414 (2001) 359-367.
[2] M. M. Thackeray, W. I. F. David, P. G. Bruce, J. B. Goodenough, Mater. Res. Bull., 18 (1983) 461-472.
[3] L. L. Peng, Y. Zhu, U. Khakoo, D. H. Chen, G. H. Yu, Nano Energy., 17 (2015) 36−42.
[4] J. Feng, X. Gao, L. Cia, S. Xiong, RSC Adv., 6 (2016) 7224-7228.
[5] J. Wang, Y. Li, X. Sun, Nano Energy, 2 (2013) 443-467.
[6] A. Ratnakar, K. Hari Prasad, S Vivekananthan, P C Karthika, Aashutosh Kumar, Material Today: Proceedings, 3(10) (2016) 4052-4057.
[7] K. Hari Prasad, S. Vinoth, A. Ratnakar, N. Satyanarayana, Material Today: Proceedings, **3(10)** (2016) 4046-4051.
[8] K. Hari Prasad, P. Muralidharan, E.S. Srinadhu, N. Satyanarayana, Advanced Materials - TechConnect Briefs 2017, 2 (2017) 106-109.
[9] K. Hari Prasad, P. Muralidharan, E.S. Srinadhu, N. Satyanarayana, Advanced Materials - TechConnect Briefs 2017, 2 (2017) 90-93.
[10] K. Hari Prasad, P. Muralidharan, E.S. Srinadhu, N. Satyanarayana, Advanced Materials - TechConnect Briefs 2017, 2 (2017) 114-117.
[11] Kamatam Hari Prasad, S.Vintoth, P. Jena, M. Venkateswarlu, N. Satyanarayana, Materials Chemistry and Physics, **194** (2017) 188-197.
[12] Kamatam Hari Prasad, S. Subramanayam, T.N. Sai ram, G. Amarendra, E.S. Srinadh, N. Satyanarayana, Journal of Alloys and Compounds, **718** (2017) 459-470.
[13] K. Hari Prasad, A. Ratnakar, Aashutosh Kumar, N. Satyanarayana, Material Today: Proceedings, **3(10)** (2016) 4064-4069.
[14] Paramananda Jena, N. Nallamuthu, K. Hariprasad, M. Venkateswarlu, N. Satyanarayana, Journal of Sol-gel Science and Technology, **72** (2014) 480-489.
[15] K. Hari Prasad, N. Naresh, B. Nageswar Rao, M. Venkateswarlu, N. Satyanarayana, Material Today: Proceedings, **3(10)** (2016) 4040-4045.
[16] P. Muralidharan, N. Nallamuthu, I. Prakash, N. Satyanarayana, J. Am. Ceram. Soc., 90 (2007) 125-131.